From the prediction of tunneling hazards to point-source seismic amplitude versus offset, the March-April 2008 issue of GEOPHYSICS has something of interest for you.

Tunneling hazards. In a challenging urban environment, Martí et al. use vibroseis-based first-arrival traveltime tomography to determine potential hazards for a new Barcelona subway extension tunnel. Outcrop data and core samples combined with traveltime seismic tomography provide a distribution of the main faults and dikes that might intersect the proposed tunnel (Figure 1). High permeability from the intersections of fractures and dikes create drilling risks by creating groundwater flow paths.

Modeling migration. Starting with an impedance model, Toxopeus et al.'s multidimensional algorithm simulates modeling followed by migration. The algorithm honors the multidimensional wavelet that resides in migrated seismic data. Compare the migrated data (Figure 2, top) with both the output of the authors' combined modeling and migration algorithm (Figure 2, middle) and with the result of 1D convolution modeling of an impedance model for that data (Figure 2, bottom). As the authors note, horizontal smearing by the multidimensional operator acting on the impedance model is a necessary ingredient in interpreting the observed data.

Nonunique inverses. Many inversion problems do not have unique inverses. Blaschek et al. address this ambiguity for inversion of induced polarization data from a hydrogeologic test site in Krauthausen, Germany. The top row of Figure 3 illustrates the results of an inversion with a smoothness constraint. Additional rows illustrate inversion results for increasing the reward for a blocky model. All these inversion models equally satisfy the observed data.

Interpolation. In addition to using the recorded data values, While et al.'s interpolation scheme uses field-recorded spatial derivatives. Interpolation allows economic, coarse acquisition line spacing while simultaneously avoiding unwanted spatial aliasing. Theoretically, the addition of the band-limited, field-recorded spatial derivatives allows for a factor-of-three increase in the unaliased line spacing in comparison with interpolating only amplitude values without field-recorded spatial derivatives. However, edge effects and other considerations reduce this to a factor-of-two increase.

The authors apply their interpolation method to gravity gradient data. Figure 4 shows the original gravity data recorded at the Australian Cannington ore deposit, along with results from a cubic interpolation and from their own interpolation methods.

Pairwise seismic inversion. From the expected shapes for amplitude spectra of pairs of reflection coefficients, Puryear and Castagna determine the timing, separations, and values of those reflection coefficients for reflection-pair separations. By employing this methodology in a window that progresses down the trace, the authors estimate sequential pairs of reflection coefficients. By rotating the phase of these reflection coefficients, the authors create impedancelike sections with the resolution limit of one-half the tuning thickness.

Figure 5b shows the comparison of such data with a similarly phase-rotated original data.

GPR geometric attributes. As used by McClymont et al., geometric attributes of 3D ground-penetrating-radar data (Figure 6) assist in visualizing New Zealand's Alpine Fault Zone. The

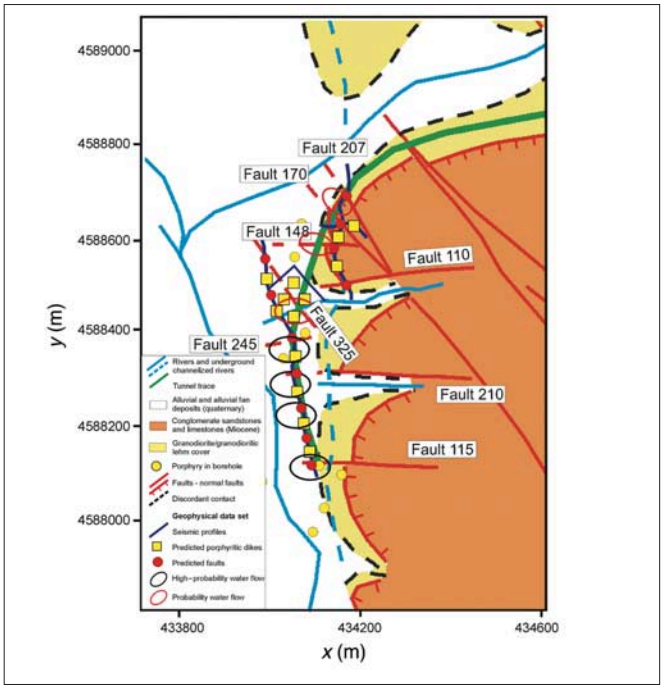

Figure 1. *Identification of the most probable groundwater flow paths along the proposed subway tunnel path (black and red circles) (Figure 8 from "High-resolution seismic characterization in an urban area: Subway tunnel construction in Barcelona, Spain," by Martí et al.).*

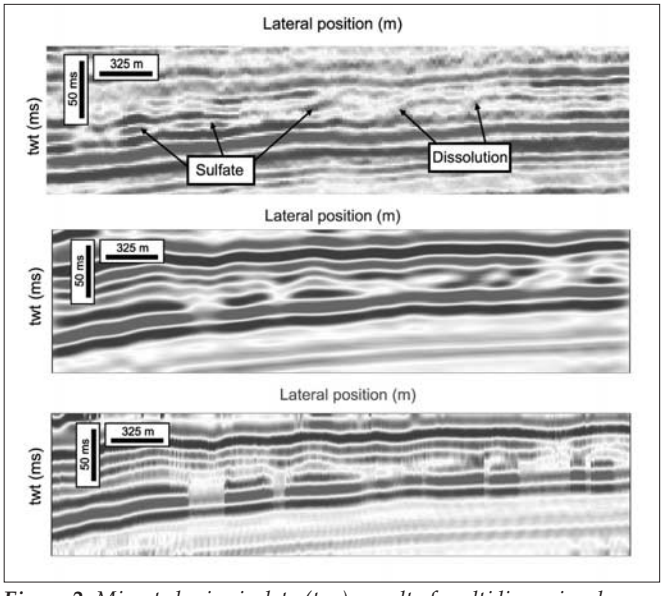

Figure 2. *Migrated seismic data (top), result of multidimensional model (middle), and result of 1D modeling (bottom) (Figures 9, 11, and 12 from "Simulating migrated and inverted seismic data by filtering a geologic model," by Toxopeus et al.).*

contrast attribute better defines recent shallow-dipping fluvial sediments. Within a small analysis volume, the contrast attribute measures the differences in amplitude of adjacent data values in a specified direction. Continuous horizontal reflections transform to low-contrast values when measured in the horizontal (x or y) direction and to high-contrast values when measured in the depth (z) direction.

The homogeneity attribute shown in Figure 6 is a measure of the similarity of adjacent amplitudes perpendicular to the plane of the cross-section (y direction) and highlights con-

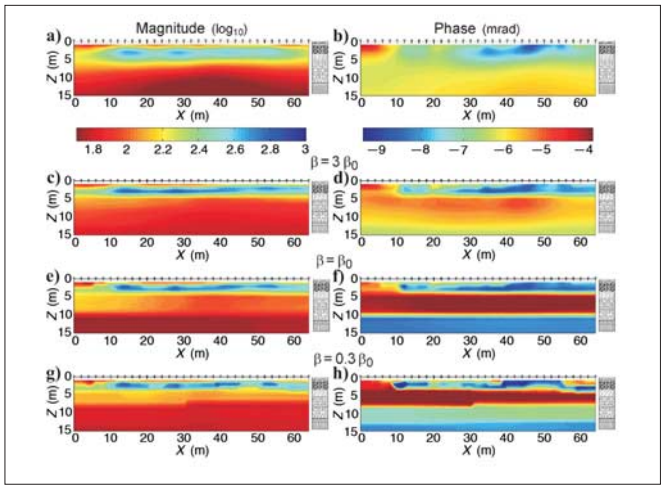

Figure 3. *Inversion of 0.3-Hz induced polarization data with decreasing amounts of smoothing. The identical right columns illustrate the lithology obtained from wells at the test site (Figure 10 from "A new sensitivity-controlled focusing regularization scheme for the inversion of induced polarization data based on the minimum gradient support," by Blaschek et al.).*

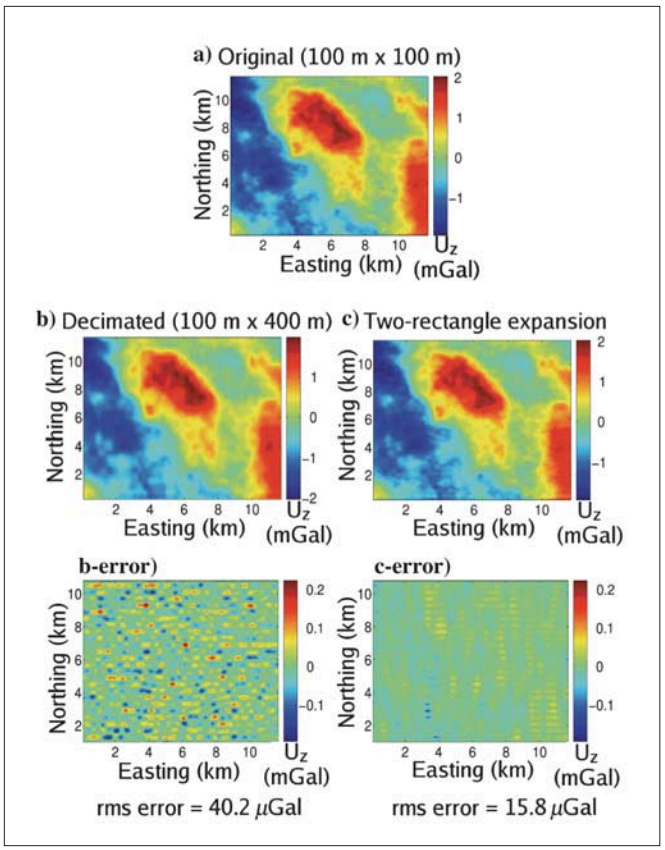

Figure 4. *Vertical gravity data from Cannington ore deposit in Australia (top). Data after decimation and cubic interpolation (middle left) and after interpolation with the addition of gradient data (middle right.) The lower pair shows the difference between original data and respective interpolated data (detail from Figure 9 from "Interpolation of gravity and gravity gradient data by using the generalized sampling expansion: Theory," by While et al.).*

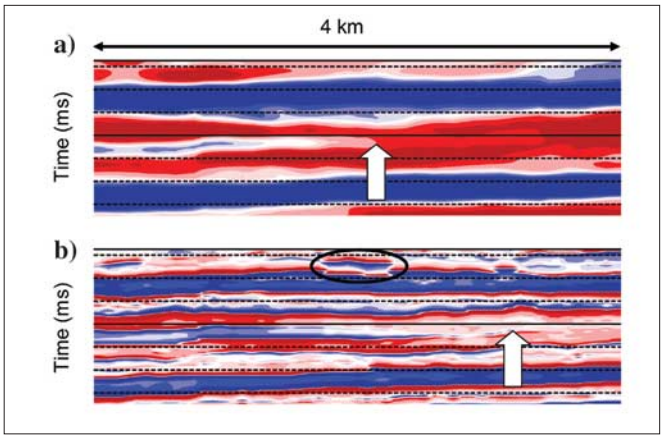

Figure 5. *(a) –90° phase rotation of original seismic data; (b) –90° phase rotation of the authors' inverted reflection-coefficient data (Figure 20 from "Layer-thickness determination and stratigraphic interpretation using spectral inversion: Theory and application," by Puryear and Castagna).*

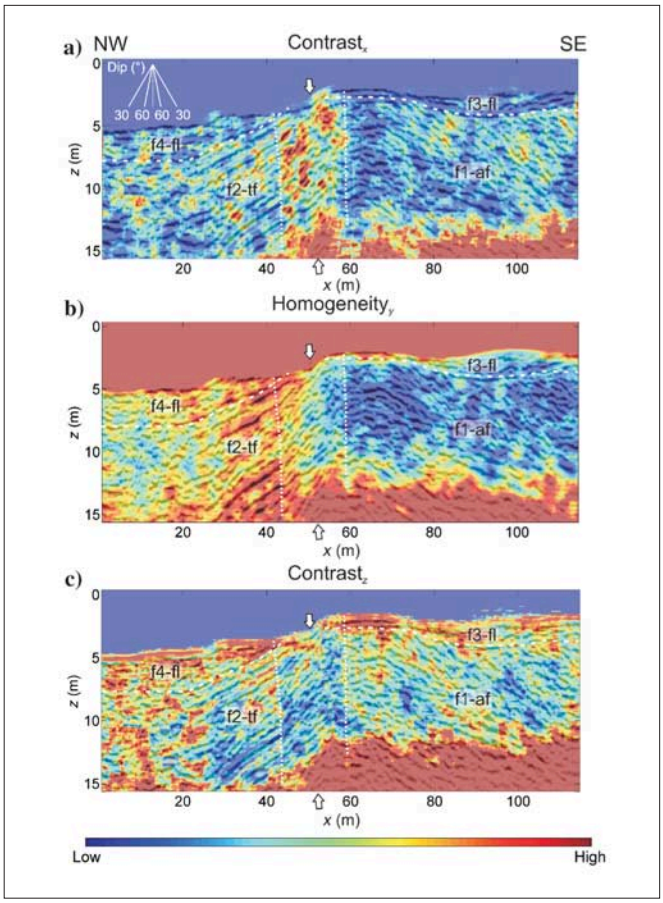

Figure 6. *Contrast and homogeneity structural attributes extracted from 3D GPR data acquired over the New Zealand Alpine Fault. Note that the upper and lower figures are the contrast attributes calculated in the inline (x) and depth (z) directions (Figure 12 from "Visualization of active faults using geometric attributes of 3D GPR data: An example from the Alpine Fault Zone, New Zealand," by McClymont et al.).*

tinuous reflections that parallel the fault plane.

Spherical-wave AVO. Through use of a Plexiglas reflector submerged in a water tank, Alhussain et al. experimentally verify spherical-wave AVO response. Their laboratory model simulates a 22-Hz dominant-frequency source wavelet reflecting from an interface 2.4 km deep.

Experimental and theoretical results demonstrate that the AVO deviates from the plane-wave Zoeppritz solution at large angles (Figure 7). To paraphrase the authors, at any given point

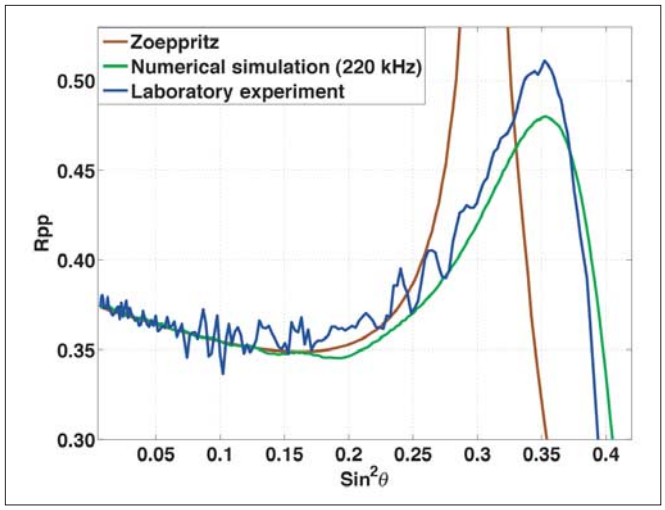

Figure 7. *Angular-dependent, point-source reflection coefficients for a water-Plexiglas interface. The graph compares results of the laboratory experiment with a plane-wave Zoeppritz analytic solution and a point-source numerical simulation (Figure 3 from "Experimental verification of spherical-wave effect on the AVO response and implications for three-term inversion," by Alhussain et al.).*

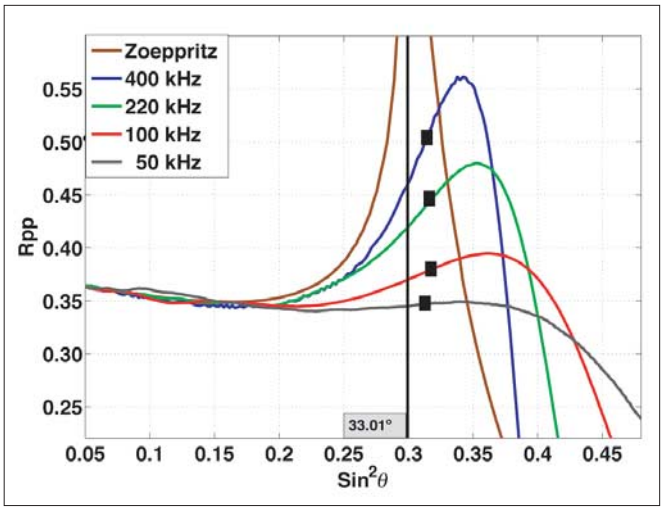

Figure 8. *Numerically calculated point-source, frequency-dependent AVA (Figure 4 from "Experimental verification of spherical-wave effect on the AVO response and implications for three-term inversion," by Alhussain et al.).*

of the interface, the reflection of the spherical wave includes both reflections from the plane wave corresponding to the specular ray and a collection of plane waves corresponding to the ray beam around the central ray. We might think of the amplitude of the reflected wave as an average of plane-wave reflection coefficient over a range of incident angles around the ray angle.

To paraphrase the authors again, the frequency-dependence of the AVO (Figure 8) depends on the averaging aperture, which is controlled by the size of the Fresnel zone (and thus depends on both the frequency and the distance between the source and the interface).

Although the authors note that the spherical-wave effect contaminates the classic three-parameter inversion for V_P, V_S, and density, they present an alternative approach for estimation of those parameters. TLE

—*Stephen J. Hill*
Colorado School of Mines